Democratic Joint Operations Algorithm for Optimal Power Extraction of PMSG based Wind Energy Conversion System

Bo Yang[a], Tao Yu[b,*], Hongchun Shu[a], Xiaoshun Zhang[c], Kaiping Qu[b], Lin Jiang[d]

[a] *Faculty of Electric Power Engineering, Kunming University of Science and Technology, 650500 Kunming, China*

[b] *College of Electric Power, South China University of Technology, 510640 Guangzhou, China*

[c] *Department of Electrical Engineering, The Hong Kong Polytechnic University, Hong Kong*

[d] *Department of Electrical Engineering & Electronics, University of Liverpool, Liverpool, L69 3GJ,United Kingdom*

***Abstract*--This paper proposes a novel military philosophy inspired meta-heuristic algorithm called democratic joint operations algorithm (DJOA), which attempts to find the optimal parameters of proportional-integral-derivative (PID) controllers of permanent magnetic synchronous generator (PMSG) based wind energy conversion system (WECS), such that a maximum power point tracking (MPPT) under different wind speed profiles can be achieved. In order to realize a deeper optimum search, an additional deputy officer is introduced into the democratic defensive operations of each military unit, in which the soldiers can wisely seek a more optimal defensive position following the consensus/compromise of the officer and deputy officer. Furthermore, the shuffling strategy of shuffled frog leaping algorithm (SFLA) is employed for the shuffling regroup operations of DJOA, which effectively avoids the local optimum trapping by sharing the global position information among all the soldiers. Three case studies are carried out, e.g., step change of wind speed, low-turbulence stochastic wind speed variation, and high-turbulence stochastic wind speed variation, respectively. Simulation results verify that an improved optimal power extraction can be realized by DJOA compared with that of other five typical meta-heuristic algorithms.**

***Keywords* -- Democratic joint operations algorithm; Shuffling strategy; Permanent magnetic synchronous generator; Maximum power point tracking; Wind energy conversion system**

Nomenclature

Variables		J_{tot}	total inertia of the drive train
v_{wind}	wind velocity	p	pole pairs
ρ	air density	D	damping coefficient
R	turbine radius	v'_{sd},v'_{sq}	dq-axis compensation terms
C_P	power coefficient	*Abbreviations*	
C_{Pmax}	maximum power coefficient	**PMSG**	permanent magnetic synchronous generator
λ	tip-speed-ratio	**GA**	genetic algorithm
λ_{opt}	optimal tip-speed-ratio	**PSO**	particle swarm optimization
β	blade pitch angle	**WECS**	wind energy conversion system
T_e	electromagnetic torque	**JOA**	joint operation algorithm
T_m	mechanical torque	**DJOA**	democratic joint operation algorithm
Q_s	stator reactive power	**PID**	proportional-integral-derivative
P_s	stator active power	**QGA**	quantum genetic optimization algorithm
ω_s	synchronous angle speed	**MPPT**	maximum power point tracking

* Corresponding author: Tel:+86 13002088518.
E-mail address:taoyu1@scut.edu.cn (T. Yu).

ω_r	rotor angular speed	**BLPSO**	biogeography-based learning particle swarm optimization
ω_b	electrical base speed	**AG**	approximate gradient
i_{dr}, i_{qr}	dq-axis rotor currents	**SLFA**	shuffled frog leaping algorithm
i_{ds}, i_{qs}	dq-axis stator currents	***PID Control Parameters***	
V_d, V_q	dq-axis control inputs	K_{P1}	proportional gain of rotor speed
T_e	electromagnetic torque	K_{I1}	integral gain of rotor speed
Ψ_{sd},Ψ_{sq}	dq-axis fluxes	K_{D1}	derivative gain of rotor speed
Ψ_f	flux linkage	K_{P2}	proportional gain of q-axis current
System Parameters		K_{I2}	integral gain of q-axis current
σ	the leakage coefficient	K_{D2}	derivative gain of q-axis current
R_s,R_r	stator and rotor resistances	K_{P3}	proportional gain of d-axis current
L_s,L_r	stator and rotor inductances	K_{I3}	integral gain of d-axis current
L_m	magnetizing inductance	K_{D3}	derivative gain of d-axis current

1. Introduction

In the past decade, the astonishing global population booming and continuous fossil fuel depletion have driven considerable social and industrial demands of renewable energy, e.g., solar, wind, hydro, tidal, biomass, geothermal, ect., among which wind energy conversion system (WECS) deployment is in an amazingly fast expansion, whether onshore or offshore, given the promising economic merits of wind power and the increased competitiveness regarding other sources of electrical energy [1]. So far, WECS mainly contains two groups of generators, i.e., doubly-fed induction generator (DFIG) [2] and permanent magnet synchronous generator (PMSG) [3]. Currently, the application of PMSG has been noticeably increased thanks to its elegant advantages of simple structure, efficient energy production, gearless construction, self-excitation, and low noise [4]. In practice, a major task of PMSG controller is to extract the mechanical power at various wind speed as much as possible, also known as maximum power point tracking (MPPT) [5]. At the moment, conventional vector control (VC) using classical proportional-integral-derivative (PID) loops are widely employed to design the control system of PMSG with the prominent features of operation reliability and structure simplicity [6]. Although fractional-order PI/PID control could be employed to improve the dynamical performance by introducing two additional control parameters [7], one inherent weakness of such control framework is its inconsistent control performance when operation condition varies due to the one-point linearization, such issue becomes especially severe in the face of PMSG as wind speed usually changes in a highly stochastic and fast time-varying pattern [8].

Generally speaking, two main types of methodology have continuously endeavoured to tackle this thorny obstacle, e.g., nonlinear robust/adaptive control and meta-heuristic algorithms. The former one aims to fully/partially remove the system nonlinearities to achieve a globally consistent control performance or to introduce various robust/adaptive mechanisms to efficiently handle the unmodelled dynamics, parameter uncertainties, external disturbances, etc. [9]. In references [10,11], a feedback linearization control (FLC) was proposed to fully compensate all system nonlinearities of PMSG for MPPT, which however requires an accurate system model. In order to enhance system robustness against modelling uncertainties and to improve total harmonic distortion property, a sliding-mode control (SMC) scheme was designed with an enhanced exponential reaching law [12]. Moreover, a nonlinear Luenberger-like observer was employed to estimate the mechanical variables by only the measurement of electrical variables of PMSG to achieve MPPT [13]. Besides, an artificial neural network (ANN)-based reinforcement learning (RL) was adopted to enable the PMSG to behave like an intelligent agent with memory to learn from its own experience, thus the MPPT learning efficiency could be greatly improved [14]. In addition, a nonlinear backstepping approach based on Lyapunov theory was reported in reference [15], which is able to accurately track the optimal power curve under various wind speed. Furthermore, an active disturbance rejection control (ADRC) scheme was devoted to reject both the internal and external disturbances of PMSG to capture the maximum power from the wind [16].

On the other hand, an enormous variety of meta-heuristic algorithms have been proposed with different variants/modifications to resolve plenty of complex and complicated management or engineering problems, which are, in essence, inspired from the millions year of extraordinarily competitive biological evolution in the harsh nature (evolutionary algorithm) or elaborately emulate the efficient collective behaviours of animals, insects, or human society (swarm-based algorithm) [17]. A genetic algorithm (GA) was applied on PMSG to optimally adjust proportional-integral (PI) control parameters considering both symmetrical and unsymmetrical faults, as well as the permanent fault condition due to unsuccessful reclosing of circuit breakers [18]. In work [19], a particle swarm optimization (PSO) was used to improve the control performance of PMSG under various wind speed via tuning the PI control parameters. Besides, a firefly algorithms (FA) was studied for the optimal PID control parameters tuning of pitch angle controller of PMSG, such that a stable and optimal power tracking could be realized [20]. Additionally, an adaptive ant colony optimization (AACO) was incorporated with general regression neural network for MPPT of WECS [21]. Meanwhile, a modified honey bee mating optimization (HBMO) algorithm was investigated for the optimal placement of renewable electricity generators, in which the transmission losses, costs of electrical generation and voltage deviation of photovoltaic units, wind turbine and fuel cell units are simultaneously considered [22]. Moreover, literature [23] reported a gradient-based multi-objective optimization algorithm using nonlinear mathematical programing to solve the multi-objective wind farm layout optimization. Besides, a bacterial foraging algorithm (BFA) was employed which attempts to accommodate high penetrations of wind power with the integration of battery energy storage system based on an economic dispatch model [24].

Thus far, how to effectively and efficiently obtain the global optimum of practical engineering problems still remains to be an extremely challenging and crucial task due to the ubiquitous difficulties of high dimensionality, multimodality, non-differentiability, and ill-conditioning. Recently, a human society behaviour inspired meta-heuristic algorithm called joint operations algorithm (JOA) has been developed to meticulously mimic the military philosophy of joint operations of multiple military units in battles, of which three important operations, e.g., offensive operations (global exploration), defensive operations (local exploitation), and regroup operations (re-organization strategy), are introduced to cooperatively deal with the annoying dilemma when the optimization algorithms are trapped at local optimum [25]. Based on the aforementioned principle, this paper proposes a novel democratic joint operations algorithm (DJOA), which aims to further enhance the global exploration ability and local exploitation ability of the original JOA associated with the following two promising characteristics:

- A democratic defensive operations is formed via the introduction of an additional deputy officer into each military unit, such that a deeper optimum search can be realized;
- A shuffling regroup operations is constructed by the use of shuffling strategy of shuffled frog leaping algorithm (SFLA) [26,27], which can further reduce the possibility of local optimum trapping.

DJOA is applied on PMSG based WECS to achieve MPPT under various wind speed profiles through optimal PID control parameters tuning. Three scenarios, such as step change of wind speed, low-turbulence stochastic wind speed variation, and high-turbulence stochastic wind speed variation, are undertaken to thoroughly evaluate the performance of DJOA and compared to that of some typical meta-heuristic algorithms.

Note that JOA [25] is a very new and effective optimization algorithm which has just been published in 2016. To the authors' best understanding and knowledge, this is the first modification and application of JOA so far. The original contribution and novelty of this paper can be summarized into the following four folds:

- In evolutionary computation domain, the concept of democracy inspired from the social science (military philosophy) [32,33] has been incorporated into DJOA to form a democratic defensive operations, while the mechanism of shuffling strategy motivated by animal behaviour (shuffled frog-leaping) [26,27] has also been employed to from a shuffling regroup operations, such that a proper exploration and exploitation can be effectively achieved. Besides, both the social science and animal behaviour mechanisms are collaboratively introduced into meta-heuristic optimization algorithms, which can be regarded as a novel interdisciplinary research between social science, biology, and evolutionary computation;

● In application domain, the MPPT of PMSG is a very crucial task in wind energy conversion. The studied PMSG model is the most widely adopted and well accepted PID control framework in both industry and academics [6]. The optimized PID control parameter by DJOA can significantly increase the wind energy extraction, which can be treated as another original contribution of interdisciplinary study between renewable energy, optimization, and control;
● In algorithm justification domain, both the PMSG model (e.g., 9 dimensions) and thirteen benchmark functions [48] (e.g., from 30 to 300 dimensions) have been investigated to fully evaluate the performance of DJOA against to that of other typical algorithms. Moreover, modified versions of the typical optimization algorithms are used which adopt the local search enhancement mechanism, such that a fair comparison of all the studied algorithms can be achieved;
● In environmental protection domain, DJOA can extract higher wind power from various wind speed compared to that of other typical algorithms, such that a large amount of free electricity can be generated. Moreover, the emission of green house gases, such as CO_2, NO_2, SO_2, can be considerably reduced into the environment.

The remaining of this paper is organized as follows. The PMSG based WECS is modelled in Section 2. Section 3 is devoted to develop the DJOA. In Section 4, the DJOA design of optimal PID control parameters tuning of PMSG for MPPT is provided. Case studies are carried out in Section 5. Several experiments on different benchmark functions are provided in Section 6. At last, Section 7 concludes the whole paper.

2. Modelling of PMSG based WECS

The configuration of a PMSG based WECS through back-to-back voltage source converter (VSC) is schematically depicted by Fig. 1, in which the wind energy captured by a variable speed wind turbine is transmitted to a gearless PMSG. In particular, the active power and reactive power of PMSG is regulated by the generator-side VSC, while the grid-side VSC attempts to deliver the generated active power to the power grid via the DC-link and to maintain the DC-link voltage [28]. Since the MPPT of PMSG mainly relies on the control of the generator-side VSC, the dynamics of grid-side VSC is ignored.

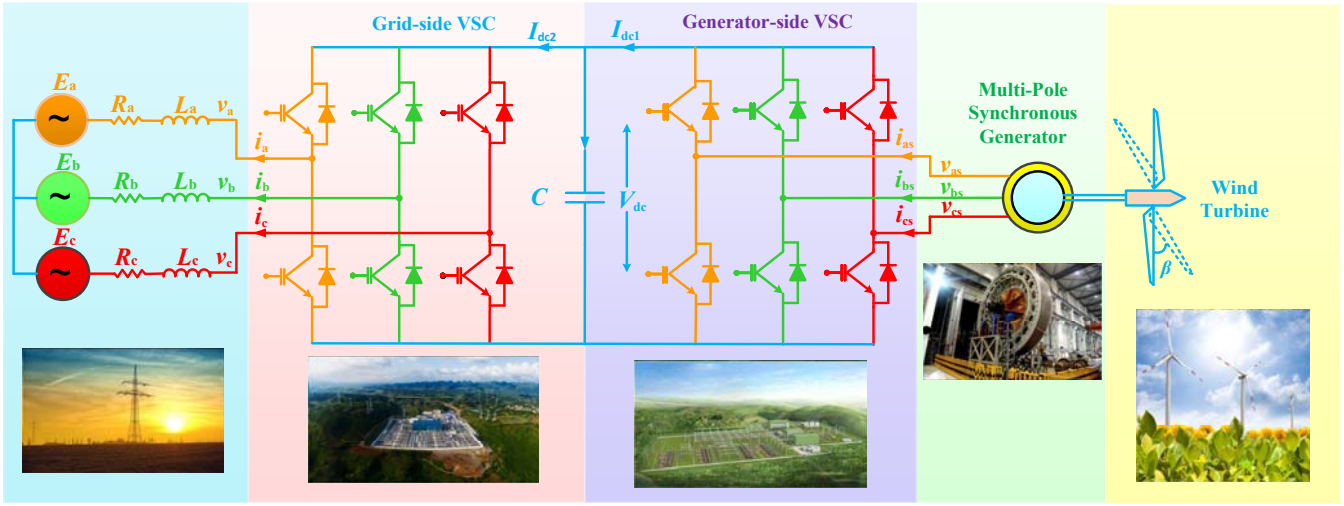

Figure 1: The configuration of a grid connected PMSG based WECS.

2.1 Variable speed wind turbine modelling

In general, the aerodynamics of wind turbine can be described by a power coefficient $C_p(\lambda,\beta)$, which is usually an algebraic function of both blade pitch angle β and tip-speed-ratio λ, with λ being defined by

$$\lambda = \frac{\omega_m R}{v_{wind}} \tag{1}$$

where ω_m denotes the mechanical rotation speed of wind turbine and v_{wind} represents the wind speed; R is the blade radius of wind turbine. According to the wind turbine dynamics, a generic equation describing the power coefficient can be written as

$$C_p(\lambda,\beta) = c_1\left(\frac{c_2}{\lambda_i} - c_3\beta - c_4\right)e^{-\frac{c_5}{\lambda_i}} \tag{2}$$

with

$$\frac{1}{\lambda_i} = \frac{1}{\lambda + 0.08\beta} - \frac{0.035}{\beta^3 + 1} \tag{3}$$

where the coefficients c_1 to c_5 are selected as c_1=0.22, c_2=116, c_3=0.4, c_4=5, and c_5=12.5, respectively [10,29].

Moreover, the mechanical power extracted by the wind turbine from the wind energy is calculated by

$$P_{\mathrm{m}} = \frac{1}{2}\rho\pi R^2 C_{\mathrm{p}}(\lambda, \beta) v_{\mathrm{wind}}^3 \tag{4}$$

where ρ is the air density. Note that during MPPT the wind turbine only operates in the sub-rated speed range while its pitch control is deactivated for the whole operation of PMSG [30].

2.2 Permanent magnetic synchronous generator modelling

A generic PMSG model based on the stator voltage equations [6] is written in the form of

$$\begin{pmatrix} v_{\mathrm{sd}} \\ v_{\mathrm{sq}} \end{pmatrix} = -R_{\mathrm{s}} \begin{pmatrix} i_{\mathrm{sd}} \\ i_{\mathrm{sq}} \end{pmatrix} - \frac{\mathrm{d}}{\mathrm{d}t} \begin{pmatrix} \Psi_{\mathrm{sd}} \\ \Psi_{\mathrm{sq}} \end{pmatrix} + \omega_{\mathrm{e}} \begin{pmatrix} 0 & -1 \\ 1 & 0 \end{pmatrix} \begin{pmatrix} \Psi_{\mathrm{sd}} \\ \Psi_{\mathrm{sq}} \end{pmatrix} \tag{5}$$

where R_{s} is the resistance of the stator winding; v_{sd}, v_{sq}, i_{sd}, i_{sq}, Ψ_{sd}, and Ψ_{sq} are the d-q components of instantaneous stator voltages, currents and fluxes, respectively. In addition, $\omega_{\mathrm{e}} = p\omega_{\mathrm{m}}$ is the electrical rotation speed. If the d-axis is aligned along the rotor-flux direction, the stator flux linkages can be calculated as

$$\begin{pmatrix} \Psi_{\mathrm{sd}} \\ \Psi_{\mathrm{sq}} \end{pmatrix} = \begin{pmatrix} L_{\mathrm{ls}} + L_{\mathrm{dm}} & 0 \\ 0 & L_{\mathrm{ls}} + L_{\mathrm{qm}} \end{pmatrix} \begin{pmatrix} i_{\mathrm{sd}} \\ i_{\mathrm{sq}} \end{pmatrix} + \begin{pmatrix} \Psi_{\mathrm{f}} \\ 0 \end{pmatrix} \tag{6}$$

where L_{ls} is the leakage inductance of the stator winding; L_{dm} and L_{qm} are the dq-axis mutual inductances between stator and rotor; Ψ_{f} is the flux linkage produced by the permanent magnet. Substitute Eq. (6) into Eq. (5), the stator voltage can be represented by

$$\begin{pmatrix} v_{\mathrm{sd}} \\ v_{\mathrm{sq}} \end{pmatrix} = -R_{\mathrm{s}} \begin{pmatrix} i_{\mathrm{sd}} \\ i_{\mathrm{sq}} \end{pmatrix} - \frac{\mathrm{d}}{\mathrm{d}t} \begin{pmatrix} L_{\mathrm{d}} i_{\mathrm{sd}} \\ L_{\mathrm{q}} i_{\mathrm{sq}} \end{pmatrix} + \omega_{\mathrm{e}} \begin{pmatrix} -L_{\mathrm{q}} i_{\mathrm{sq}} \\ L_{\mathrm{d}} i_{\mathrm{sd}} + \Psi_{\mathrm{f}} \end{pmatrix} \tag{7}$$

where $L_{\mathrm{d}} = L_{\mathrm{ls}} + L_{\mathrm{dm}}$ and $L_{\mathrm{q}} = L_{\mathrm{ls}} + L_{\mathrm{qm}}$. Under the steady-state condition, system (7) can be reduced to

$$\begin{pmatrix} V_{\mathrm{sd}} \\ V_{\mathrm{sq}} \end{pmatrix} = \begin{pmatrix} -R_{\mathrm{s}} & -\omega_{\mathrm{e}} L_{\mathrm{q}} \\ \omega_{\mathrm{e}} L_{\mathrm{d}} & -R_{\mathrm{s}} \end{pmatrix} \begin{pmatrix} I_{\mathrm{sd}} \\ I_{\mathrm{sq}} \end{pmatrix} + \begin{pmatrix} 0 \\ \omega_{\mathrm{e}} \Psi_{\mathrm{f}} \end{pmatrix} \tag{8}$$

where V_{sd}, V_{sq}, I_{sd}, and I_{sq} are the d-q components of the steady-state stator voltages and currents, respectively. The electromagnetic torque T_{e}, stator active power P_{s}, and reactive power Q_{s} are given as follows

$$T_{\mathrm{e}} = p\left(\Psi_{\mathrm{sd}} i_{\mathrm{sq}} - \Psi_{\mathrm{sq}} i_{\mathrm{sd}}\right) = p\left(\Psi_{\mathrm{f}} i_{\mathrm{sq}} + \left(L_{\mathrm{d}} - L_{\mathrm{q}}\right) i_{\mathrm{sd}} i_{\mathrm{sq}}\right) \tag{9}$$

$$P_{\mathrm{s}} = v_{\mathrm{sd}} i_{\mathrm{sd}} - v_{\mathrm{sq}} i_{\mathrm{sq}} \tag{10}$$

$$Q_{\mathrm{s}} = v_{\mathrm{sd}} i_{\mathrm{sq}} - v_{\mathrm{sq}} i_{\mathrm{sd}} \tag{11}$$

where p represents the pole pairs.

2.3 Mechanical shaft system modelling

The dynamics of mechanical shaft system and mechanical torque of PMSG are given as [10,29]

$$J_{\mathrm{tot}} \frac{\mathrm{d}\omega_{\mathrm{m}}}{\mathrm{d}t} = T_{\mathrm{m}} - T_{\mathrm{e}} - D\omega_{\mathrm{m}} \tag{12}$$

$$T_{\mathrm{m}} = \frac{1}{2}\rho\pi R^5 \frac{C_{\mathrm{p}}(\lambda,\beta)}{\lambda^3} \omega_{\mathrm{m}}^2 \tag{13}$$

where J_{tot} is the total inertia of the drive train which equals to the summation of wind turbine inertia constant and generator inertia constant; D is the viscous damping coefficient; T_{m} is the mechanical torque of the wind turbine, respectively. Moreover, electrical power is calculated as $P_{\mathrm{e}} = T_{\mathrm{e}}\omega_{\mathrm{e}}$.

2.4 MPPT profile

In order to capture the maximum wind power, the power coefficient $C_{\mathrm{p}}(\lambda,\beta)$ should be maintained at its maximum point C_{p}^{*} at various wind speed within the operation range. More specifically, maximum power coefficient C_{p}^{*} is achieved by maintaining the tip-speed-ratio λ to be equal to its optimal value λ^{*} and the pitch angle β at a fixed value, yields

$$C_{\mathrm{p}}^{*} = C_{\mathrm{p}}(\lambda^{*}) \tag{14}$$

which in turn requires the mechanical rotation speed ω_{m} to track its optimal reference ω_{m}^{*}, as follows

$$\omega_{\mathrm{m}}^{*} = \frac{v_{\mathrm{wind}}}{R}\lambda^{*} \tag{15}$$

Here, the pitch angle is taken to be $\beta = 2^{\circ}$, the optimal tip-speed-ratio $\lambda^{*} = 7.4$ while maximum power coefficient $C_{\mathrm{p}}^{*} = 0.4019$ [9,28]. Additionally, x^{*} denotes the reference of variable x throughout the whole paper.

Lastly, the aim of MPPT is to track the optimal active power curve which is obtained by connecting each maximum power point (MPP) at various wind speed [31], as briefly demonstrated by Fig. 2, with the optimal active power curve determined by

$$P_{\mathrm{opt}}(\omega_{\mathrm{m}}) = K^{*}\omega_{\mathrm{m}}^{3} \tag{16}$$

where $K^{*} = 0.5\rho\pi R^{5}C_{\mathrm{p}}^{*}/(\lambda^{*})^{3}$ denotes the shape coefficient of optimal active power, which shows that the optimal power is proportional to the cube of mechanical rotation speed and can be interpreted as the mechanical power produced on the wind turbine in terms of mechanical rotation speed.

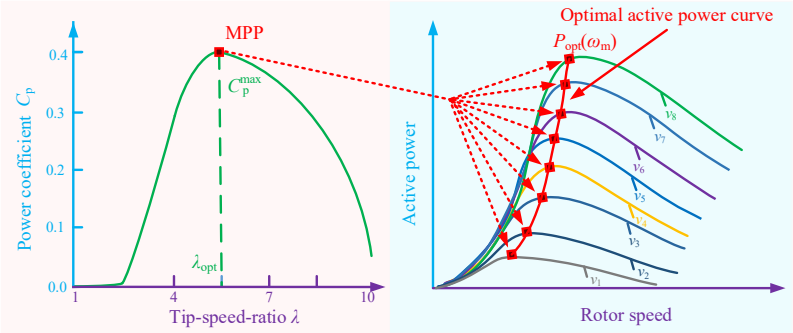

Figure 2: The optimal active power curve obtained under various wind speed.

3. Democratic Joint Operations Algorithm

JOA is basically motivated by the philosophy of military science that troops often mobilize multiple military units to participate a battle in order to win a war. It mainly contains three core strategies, i.e., offensive operations (global exploration), defensive operations (local exploitation), and regroup operations (re-organization), respectively. The former two strategies are commonly adopted in numerous meta-heuristic algorithms, however they usually contradict to each other thus the third strategy is introduced to deal with this intractable issue when JOA is trapped at a local optimum. In general, there exists a commander in the troops who dominantly instructs the overall joint operations, while each military unit contains an officer who orders the soldiers within that military unit. More details about JOA can be found to reference [25] for interested readers.

In DJOA, an additional deputy officer is employed into the original rigid single-officer governed military hierarchy in the democratic defensive operations, so a soldier's defensive position will be carefully determined by a consensus/compromise of two officers instead of a single one, as clearly shown in Fig. 3. In other words, some extent of democracy can be accomplished which attempts to largely reduce the malignant effect of misleading/wrong decision-making resulted from dictatorship during different military operations [32,33], e.g., inaccurate information, irrationality, over-confidence, espionage, etc.. Normally, the overall survival/success rate of a military unit can be considerably raised under such meticulous improvement of DJOA, that is,

a deeper optimum search can be achieved. Besides, the original regroup operations of JOA is implemented by merely a simple random permutation technique [34], which might be prone to lead an inefficient cooperation among different military units due to partial position information sharing. In order to remedy this intrinsic flaw, DJOA adopts the shuffling strategy of SFLA [26,27] to realize a shuffling regroup operations by global position information sharing among all the soldiers, such that the probability of escaping a local optimum could be dramatically increased.

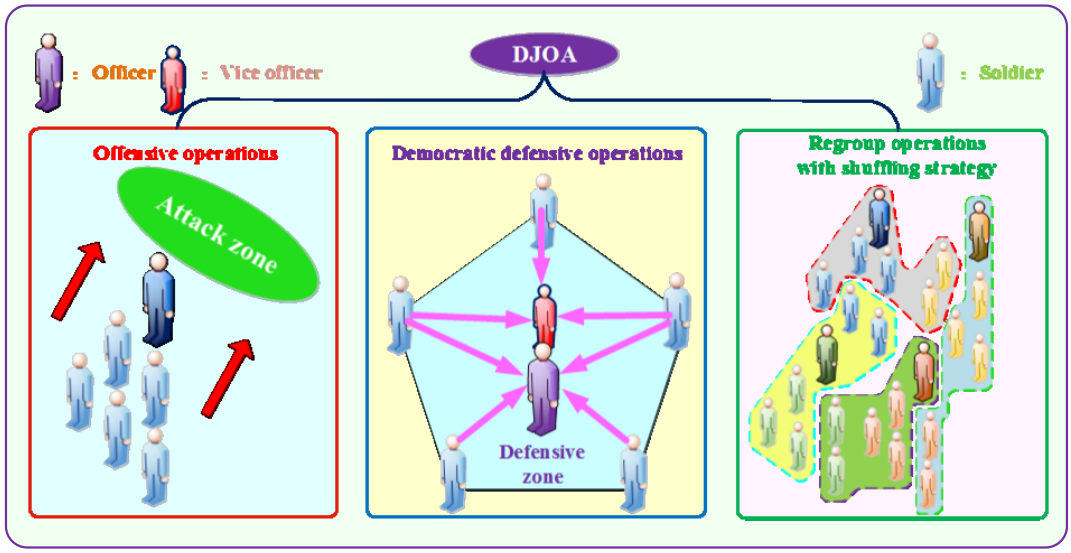

Figure 3: The schematic structure of DJOA associated with three different operations.

3.1 Initialization

At first, DJOA needs to initialize the position of every soldier in the troop, followed by dividing them into K military units where each military unit owns M soldiers. The position of the mth soldier in the kth military unit is written as $\boldsymbol{x}_m^k = (x_{m,1}^k, x_{m,2}^k, \cdots, x_{m,D}^k)$, where $m = 1, 2, \ldots, M$, $k = 1, 2, \ldots, K$. The value of the dth component $x_{m,d}^k$ of soldier $\boldsymbol{x}_m^k$ can be calculated by

$$x_{m,d}^k = L_d + \text{rand}[0,1] \times (R_d - L_d) \tag{17}$$

where rand[0,1] is a random number generated from a uniform distribution within the range of [0,1]. In addition, R_d and L_d denote the initial upper bound and lower bound of x_d, respectively. Then, the positions of officers and commander are denoted by vectors $\boldsymbol{x}_k^{\mathrm{O}}=(x_{k,1}^{\mathrm{O}}, x_{k,2}^{\mathrm{O}}, \cdots, x_{k,D}^{\mathrm{O}})$, $k = 1, 2, \ldots, K$ and $\boldsymbol{x}^{\mathrm{C}} = (x_1^{\mathrm{C}}, x_2^{\mathrm{C}}, \cdots x_D^{\mathrm{C}})$, respectively.

3.2 Offensive operations

Offensive operations are one of the most decisive factors for winning battles. Typically, a commander carefully assigns different offensive missions to the officers based on the current combat intelligence. Followed by that, the officers will order their soldiers to strictly accomplish their own missions. In order to mathematically describe the dynamical roles of commander, officers, and soldiers, it assumes that a commander always aims to guide the offensive direction of each military unit, while the offensive distance of each soldier is determined by the following two factors:

- The updated lower bound and upper bound which represent the role of officers or the current combat intelligence;
- A random number which determines the individual differences among each soldiers.

Note that the commander is one of the officers, which implies that there is a military unit uniquely affiliated with the commander. Hence, the soldiers within this military unit usually receive direct missions/orders from the commander, and update their positions consequently, as follows

$$x_{m,d}^{k}=\begin{cases} x_{m,d}^{k}+\text{rand}[0,1]\times\left(R_{d}^{k}-x_{m,d}^{k}\right), & \text{if } x_{d}^{\text{C}}>x_{m,d}^{k} \\ x_{m,d}^{k}+\text{rand}[0,1]\times\left(L_{d}^{k}-x_{m,d}^{k}\right), & \text{otherwise} \end{cases} \tag{18}$$

$$\begin{cases} L_{d}^{k}=x_{k,d}^{\text{O}}+P_{t}\times\left(L_{d}-x_{k,d}^{\text{O}}\right) \\ R_{d}^{k}=x_{k,d}^{\text{O}}+P_{t}\times\left(R_{d}-x_{k,d}^{\text{O}}\right) \end{cases} \tag{19}$$

$$P_{t}=\left|\cos(t\times F\times\pi)\right| \tag{20}$$

where x_{d}^{C} is the commander's dth position while $x_{k,d}^{\text{O}}$ means the officer's dth position of the kth military unit; $t = (1, 2, \ldots, T)$ is the current iteration and T represents the number of maximum allowable iterations; P_t represents a dynamic periodic parameter which can adjust the trade-off between global exploration and local exploitation; and F is a user-specified constant to determine the frequency of the cosine function, respectively.

If some soldiers do not belong to a military unit directly lead under a commander, their new positions will be selected as

$$x_{m,d}^{k}=\begin{cases} x_{m,d}^{k}+\text{rand}[0,1]\times\left(R_{d}^{k}-x_{m,d}^{k}\right), & \text{if } x_{d}^{\text{C}}>x_{m,d}^{\text{O}} \\ x_{m,d}^{k}+\text{rand}[0,1]\times\left(L_{d}^{k}-x_{m,d}^{k}\right), & \text{otherwise} \end{cases} \tag{21}$$

Here, it is worth noting that the only difference between position updates (18) and (21) is the guiding order of each soldier's offensive direction.

3.3 Democratic defensive operations

For each military unit, the soldiers usually endeavor to form the strongest fortifications in their occupied region to prevent any potential attacks from their enemies. In order to achieve the best defense and to ensure the personal security of both officer and deputy officer, the soldiers must seek the optimal defensive position around these two officers. Based on the aforementioned strategy, a candidate defensive position $\boldsymbol{u}_{m}^{k}=(u_{m,1}^{k}, u_{m,2}^{k}, \cdots, u_{m,D}^{k})$ of the mth soldier in the kth military unit can be obtained by

$$u_{m,d}^{k_1}=\begin{cases} x_{m,d}^{\text{O}}+P_{t}\times\text{Gaussian}\left(0,\left(x_{m,d}^{\text{O}}-x_{m,d}^{k}\right)^{2}\right), & \text{if } d=d_{\text{rand}} \text{ or } \text{rand}[0,1]\le P_{t} \\ x_{m,d}^{k}, & \text{otherwise} \end{cases} \tag{22}$$

$$u_{m,d}^{k_2}=\begin{cases} x_{m,d}^{\text{S}_1}+P_{t}\times\text{Gaussian}\left(0,\left(x_{m,d}^{\text{S}}-x_{m,d}^{k}\right)^{2}\right), & \text{if } d=d_{\text{rand}} \text{ or } \text{rand}[0,1]\le P_{t} \\ x_{m,d}^{k}, & \text{otherwise} \end{cases} \tag{23}$$

$$u_{m,d}^{k}=\frac{u_{m,d}^{k_1}+u_{m,d}^{k_2}}{2} \tag{24}$$

where $u_{m,d}^{k}$ represents the dth defensive position of the mth soldier in the kth military unit; $x_{m,d}^{\text{S}}$ is the dth defensive position of the mth soldier's deputy officer; $\text{Gaussian}\left(0,\left(x_{m,d}^{\text{O}}-x_{m,d}^{k}\right)^{2}\right)$ is a random number sampled from the Gaussian distribution with a mean value of 0 and a standard deviation $\left|x_{m,d}^{\text{O}}-x_{m,d}^{k}\right|$, which ensures that the new dth position of the mth soldier in the kth military unit could almost fall into a vicinity around $x_{m,d}^{\text{O}}$ when the condition ($d=d_{\text{rand}}$ or $\text{rand}[0,1]\le P_t$) is satisfied; and d_{rand} denotes an integer randomly generated from the set $\{1, 2, \ldots, D\}$ which is used to guarantee that at least one dimension is changed for a specific solider.

The new position of each soldier in the next iteration relies on the fitness function of the current position $\boldsymbol{x}_{m}^{k}$ and the generated candidate defensive position $\boldsymbol{u}_{m}^{k}$, gives

$$\boldsymbol{x}_{m}^{k}=\begin{cases} \boldsymbol{u}_{m}^{k}, & \text{if } f(\boldsymbol{u}_{m}^{k})<f(\boldsymbol{x}_{m}^{k}) \\ \boldsymbol{x}_{m}^{k}, & \text{otherwise} \end{cases} \tag{25}$$

Here, the above position update implies that the democratic defensive operations should bias to the local exploitation. Note that P_t can directly alter the soldiers' modified ratio of dimension and the scale of searching range (22)-(24), so as to adjust their global exploration and local exploitation. In other words, the introduction of the deputy officer (23) can achieve a deeper optimum search.

3.4 Shuffling regroup operations

When the triggering condition of regroup operations is met, the shuffling strategy [26,27] will be executed to promote a global position information sharing among all the soldiers, such that the direction searching will be converged to the most promising region identified by each military unit, as follows

$$\boldsymbol{Y^k} = \left[\left(\boldsymbol{D(m)^k},\ f(m)^k \middle| \boldsymbol{D(m)^k} = \boldsymbol{D\left(K + N(m-1)\right)}\right)\right] \tag{26}$$

$$f(m)^k = f\left(k + N(m-1)\right), m = 1, \dots, M; k = 1, \dots, K \tag{27}$$

where set $\{\boldsymbol{D(i)}, f(i), i = 1, \dots, N\}$ is the stored positions and fitness functions of all soldiers ranked in the descending order, with *i*=1 represents the soldier with the best performance value (the minimal fitness function); *M* is the population size of each military unit; *K* is the number of military units; and *N=M*K* is the total population size of all the military units, respectively.

Followed by regroup operations, DJOA will promote a new officer in each new military unit. Since the shuffling regroup operations do not need to evaluate the fitness functions of soldiers, it just requires reasonably low computational costs.

4. DJOA Design for Optimal PID Control Parameters Tuning of PMSG based WECS

In this section, the proposed DJOA will be employed for optimal PID control parameters tuning of PMSG based WECS for MPPT under various wind speed profiles.

4.1 DJOA based control structure for PMSG

A typical decoupled d-q current PID controller is given as

$$v_{\mathrm{sd}} = -\left(R_{\mathrm{s}} i_{\mathrm{sd}} + L_{\mathrm{d}} \frac{\mathrm{d}i_{\mathrm{sd}}}{\mathrm{d}t}\right) - \omega_{\mathrm{e}} L_{\mathrm{q}} i_{\mathrm{sq}} \tag{28}$$

$$v_{\mathrm{sq}} = -\left(R_{\mathrm{s}} i_{\mathrm{sq}} + L_{\mathrm{q}} \frac{\mathrm{d}i_{\mathrm{sq}}}{\mathrm{d}t}\right) + \omega_{\mathrm{e}} L_{\mathrm{d}} i_{\mathrm{sd}} + \omega_{\mathrm{e}} \Psi_{\mathrm{f}} \tag{29}$$

where the item in the bracket of (28) and (29) is regarded as the state equation between the voltage and current on d-q axis, and the other items are considered as the compensation or disturbance terms. Fig. 4 illustrates the overall DJOA based control structure of PMSG for MPPT, in which the d-q voltage references v_{sd}^* and v_{sq}^* are the sum of d-q voltages, while v'_{sd} and v'_{sq} denote the compensation items. In particular, v_{sd}^* and v_{sq}^* are used to generate the three-phase sinusoidal reference voltages to control PMSG, as shown in Eq. (30) and Eq. (31). Finally, the control inputs are modulated by the sinusoidal pulse width modulation (SPWM) technique [35].

$$v_{\mathrm{sd}}^* = v'_{\mathrm{sd}} - \omega_{\mathrm{e}} L_{\mathrm{q}} i_{\mathrm{sq}} \tag{30}$$

$$v_{\mathrm{sq}}^* = v'_{\mathrm{sq}} + \omega_{\mathrm{e}} L_{\mathrm{d}} i_{\mathrm{sd}} + \omega_{\mathrm{e}} \Psi_{\mathrm{f}} \tag{31}$$

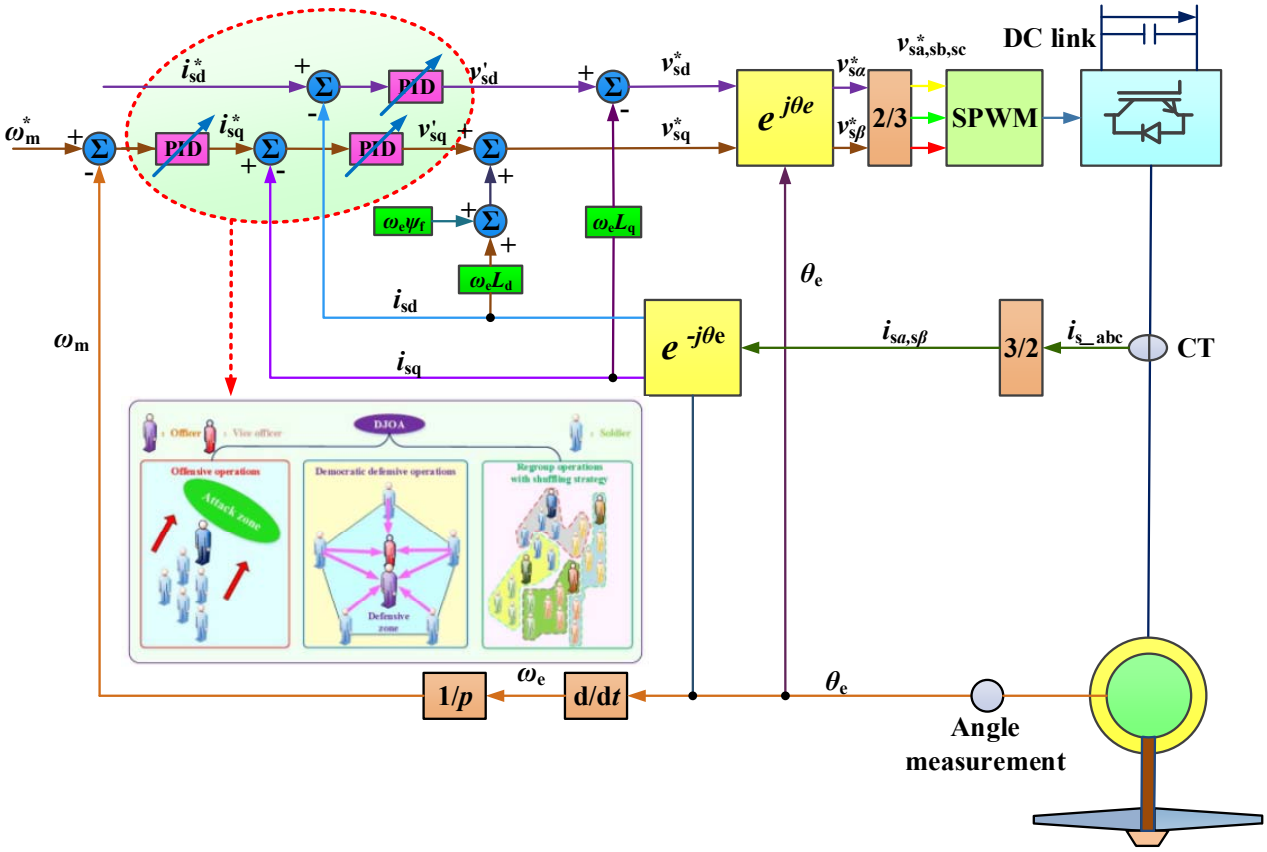

Figure 4: The overall DJOA based control structure of PMSG for MPPT.

Under such framework, three PID loops need to be optimized by DJOA to obtain an optimal control performance. Three cases are taken into account, e.g., (a) step change of wind speed; (b) low-turbulence stochastic wind speed variation; and (c) high-turbulence stochastic wind speed variation, respectively.

To this end, the optimization model of PMSG considering the control costs is developed as follows

$$\text{Minimize } f(\mathrm{x})=\sum_{\text{Three cases}}\int_0^T\left(|i_{\mathrm{sd}}-i_{\mathrm{sd}}^*|+|\omega_{\mathrm{m}}-\omega_{\mathrm{m}}^*|+\omega_1|V_{\mathrm{q}}|+\omega_2|V_{\mathrm{d}}|\right)\mathrm{d}t \tag{32}$$

$$\text{subject to } \begin{cases} K_{\mathrm{P}i}^{\min}\le K_{\mathrm{P}i}\le K_{\mathrm{P}i}^{\max} \\ K_{\mathrm{I}i}^{\min}\le K_{\mathrm{I}i}\le K_{\mathrm{I}i}^{\max} \\ K_{\mathrm{D}i}^{\min}\le K_{\mathrm{D}i}\le K_{\mathrm{D}i}^{\max} \\ v_{\mathrm{wind}}^{\min}\le v_{\mathrm{wind}}\le v_{\mathrm{wind}}^{\max}, \\ i_{\mathrm{sd}}^{\min}\le i_{\mathrm{sd}}\le i_{\mathrm{sd}}^{\max} \\ V_{\mathrm{q}}^{\min}\le V_{\mathrm{q}}\le V_{\mathrm{q}}^{\max} \\ V_{\mathrm{d}}^{\min}\le V_{\mathrm{d}}\le V_{\mathrm{d}}^{\max} \end{cases} \quad i=1,2,3 \tag{33}$$

where a total of nine PID control parameters are required to be optimally tuned which are denoted as $K_{\mathrm{P}i}$, $K_{\mathrm{I}i}$, and $K_{\mathrm{D}i}$, respectively. Moreover, they are bounded among [0, 1000], [0, 1000], and [0, 200], respectively. T is the total operation time of each case. The wind speed v_{wind} is limited between 8 m/s to 12 m/s. In addition, the weights ω_1 and ω_2 are used to scale the magnitude of control costs which are identically chosen to be 0.25 while the control costs are bounded by their corresponding limits.

4.2 Parameter setting of DJOA

In DJOA, three user-specified control parameters, i.e., the frequency of the cosine function F, the number of military units K, and the number of soldiers in each military unit M, are very crucial which need to be carefully chosen for a satisfactory

performance. All algorithms proceed till convergence (i.e., no significant change in the objective value) by the following stopping criteria:

$$|F_k - F_{k-1}| \le \varepsilon \tag{34}$$

where ε is the tolerance of convergence error, which value is chosen to be 10^{-6} in this paper; F_k and F_{k-1} represent the fitness function value of the kth iteration and (k-1)th iteration, respectively.

Remark 1. A large F will assign the DJOA to weight more on democratic offensive operations while a small value will bias DJOA to weight more on defensive operations; A large K and M will increase the global optimum searching performance but also consume longer computation time while a small value will degrade the global optimum searching performance associated with less computation time.

4.3 Overall execution of DJOA

The overall DJOA execution procedure of PMSG for MPPT is clearly illustrated by Fig. 5.

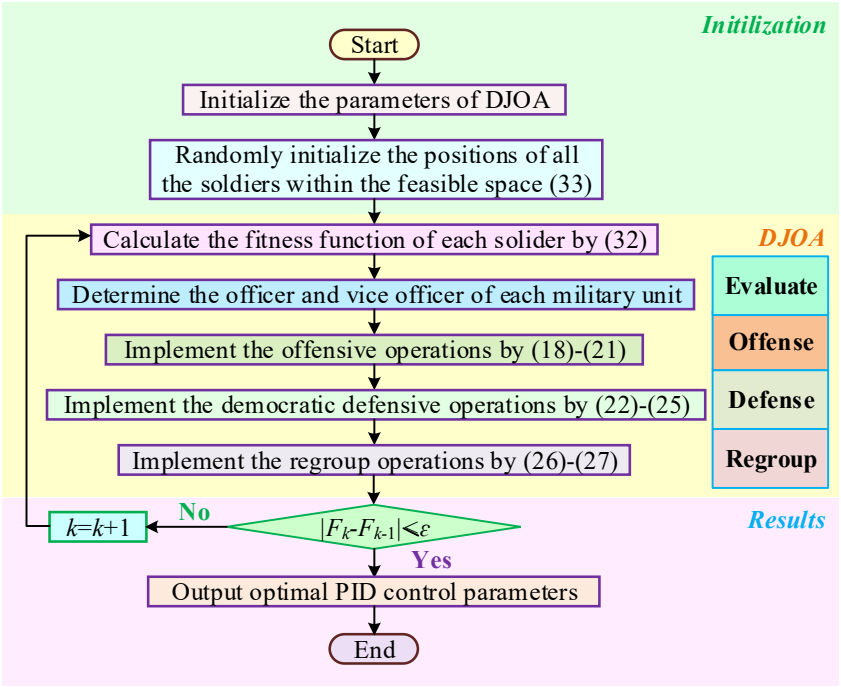

Figure 5: The overall DJOA execution procedure of PMSG for MPPT.

Remark 2. Note that the studied optimization problem, e.g., MPPT of PMSG based WECS, cannot be explicitly modelled. In other words, no function can be developed to directly describe the relationship between the nine PID control parameters and the fitness function [19-21]. Hence, the conventional optimization methods, i.e., Newton method [37], quadratic programming [38], interior-point method [39], are unable to handle this issue. As a result, this paper proposes a meta-heuristic algorithm, e.g., DJOA, as it is a model-free method.

5. Case Studies

The performance of DJOA is compared to that of five typical meta-heuristic algorithms, e.g., GA [18], quantum genetic optimization (QGA) [44], PSO [19], biogeography-based learning particle swarm optimization (BLPSO) [45] and JOA [25], together with approximate gradient (AG) [46], with all the same parameters used in these references under the aforementioned three cases. Here, original version of GA and PSO are employed. QGA exploits the power of quantum computation in order to speed up genetic procedures, in which the classical fitness evaluation and selection procedures are replaced by a single quantum

procedure. In BLPSO, each particle updates itself by using the combination of its own personal best position and personal best positions of all other particles through the biogeography-based learning migration. Such improved GA and PSO are employed to enhance their diversity mechanism and local search, such that a more fair comparison with DJOA can be made.

As the control inputs may exceed the admissible capacity of VSC at some operation point, thus their values must be limited. Here, V_q and V_d are bounded among [-0.65, 0.65] per unit (p.u.). The simulation is executed on Matlab/Simulink 7.10 using a personal computer with an Intel^R CoreTMi5 CPU at 2.2 GHz and 16 GB of RAM. The PMSG based WECS parameters are provided in Table 1. Lastly, the settings of all the applied algorithms are provided by Table 2, in which all the parameters of all algorithms are determined according to the quality of obtained optimums through trial-and-error. Note that the initial populations affect the optimization results of these meta-heuristic optimization algorithms. In order to cover the entire search domain as much as possible, several runs are undertaken to randomly generate their initial populations from the feasible space, as

$$x_{di}^0 = lb_d + r \cdot \left(ub_d - lb_d \right), \quad d = 1,2,...,D; i = 1,2,...,n \tag{35}$$

where x_{di}^0 is the initial solution of the dth controllable variable (dimension) for the ith individual; lb_d and ub_d is the lower and upper bounds of the dth controllable variable; r is a random number in the range [0, 1]; D is the number of controllable variables; and n is the population size, respectively.

Table 1 The PMSG based WECS parameters.

PMSG rated power	P_{base}	2 MW	**Field flux**	K_e	136.25 V·s/rad
Radius of wind turbine	R	39 m	**Pole pairs**	p	11
d-axis stator inductance	L_d	5.5 mH	**Air density**	ρ	1.205 kg/m^3
q-axis stator inductance	L_q	3.75 mH	**Rated wind speed**	v_{wind}	12 m/s
Total inertia	J_{tot}	10000 kg·m^2	**Stator resistance**	R_s	50 $\mu\Omega$

Table 2 The parameters of different algorithms.

	Parameter	**Value**
GA[18]	Population size N	100
	Mutation probability p_m	0.2
	Crossover probability p_c	0.8
	Generation gap g	20
	Generations k_{max}	120
QGA[44]	Population size N	120
	Rotation angle ϕ	0.01π
	Maximum number of qubits N_q	8
	Generations k_{max}	140
PSO[19]	Population size N	80
	Minimum velocity v_{min}	0.1
	Maximum velocity v_{max}	1
	Weight coefficients c_1/c_2	2/2
	Generations k_{max}	150
BLPSO[45]	Population size N	60
	Inertia weight ω	0.9-0.2,linearly decrease
	Acceleration coefficients c	1.496
	Maximum immigration and rates I	1
	Maximum emigration rates E	1
	Generations k_{max}	145
JOA[25]	Population size N	80
	Frequency of the cosine function F	0.006
	Number of military K	40
	Number of soldiers in each military unit M	15
	Generations k_{max}	160
DJOA	Population size N	80
	Frequency of the cosine function F	0.006
	Number of military K	40
	Number of soldiers in each military unit M	15
	Generations k_{max}	180

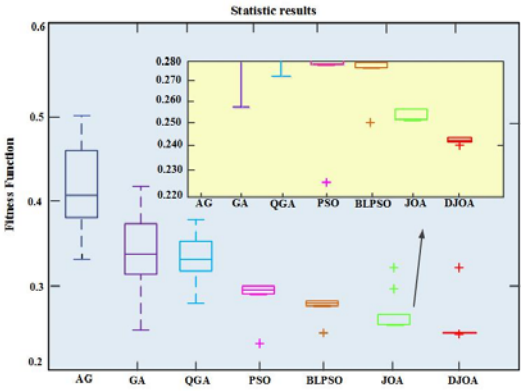

(a) solution distribution

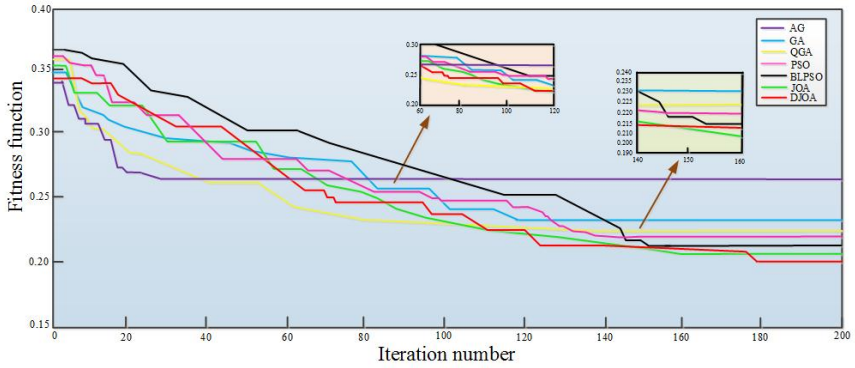

(b) algorithm convergence

Figure 6: Statistic results of different algorithms obtained in three cases.

The Box-and-Whisker plots of fitness function distribution obtained by different algorithms in 30 runs are compared in Fig. 6. It is clear that DJOA owns the highest convergence stability among four algorithms thanks to its proper trade-off between exploitation and exploration. In addition, the optimal PID control parameters found by DJOA is the best as it offers the lowest fitness function. Hence, an improved global optimum convergence of DJOA can be realized due to the incorporation of democratic defensive operations and shuffling regroup operations.

5.1 Step change of wind speed

Four consecutive step changes of wind speed increased from 8 m/s to 12 m/s with a 10 m/s^2 rate are applied to evaluate the MPPT performance of each algorithm. Meanwhile, two step changes of d-axis current reference are also adopted which aim to evaluate the d-axis current regulation performance. As shown in Fig. 7, DJOA has the smallest overshoot of active power during each MPPT, together with the highest tracking rate compared to that of other algorithms. Moreover, DJOA owns the closest power coefficient to the optimal value, which indicates that the maximum power can be effectively extracted from wind by DJOA. In contrast, AG performs the worst among all approach due to its inherent drawback of easy premature convergence. Lastly, DJOA can rapidly regulate the d-axis current with the smallest overshoot.

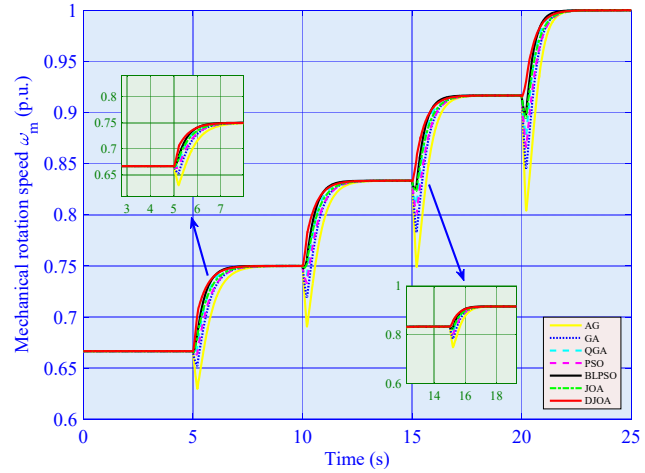

(a) mechanical rotation speed

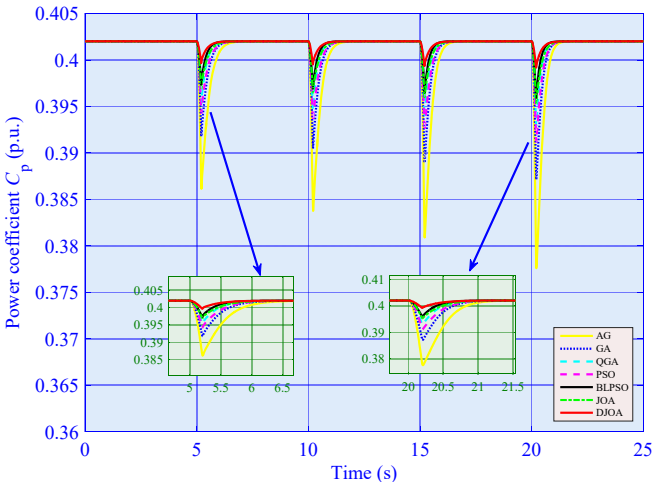

(b) power coefficient

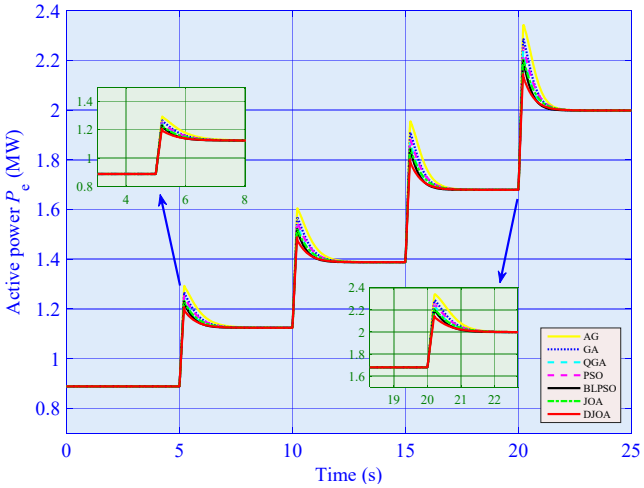

(c) active power

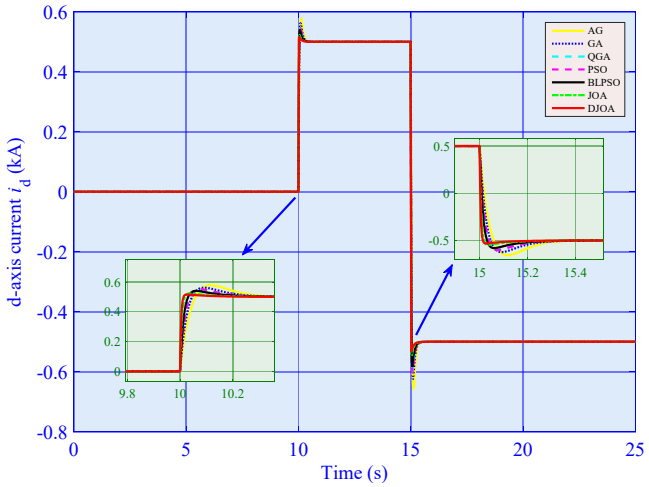

(d) d-axis current

Figure 7: System responses obtained under four consecutive step changes of wind speed from 8 m/s to 12 m/s.

5.2 Low-turbulence stochastic wind speed variation

A low-turbulence stochastic wind speed varies among 7 m/s to 11 m/s, which mimics a general wind variation, is employed to compare the control performance of each algorithms. The system responses are presented in Fig. 8, from which one can find that the power coefficient of DJOA is the optimal among all algorithms, thus DJOA can effectively achieve the MPPT in the presence of stochastic wind.

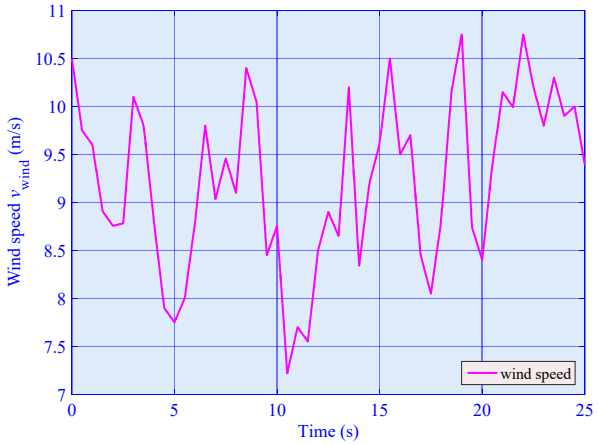

(a) wind speed profile

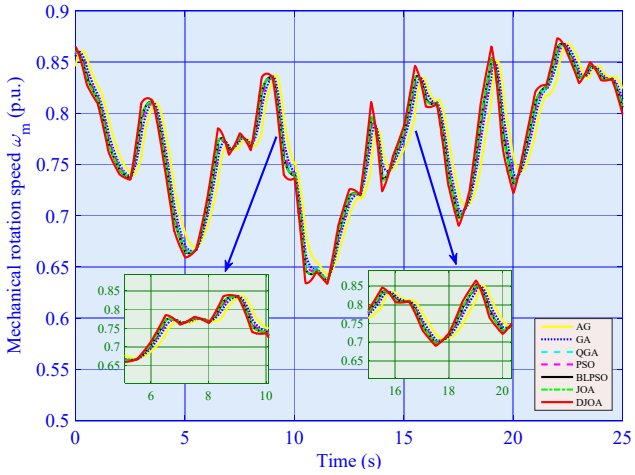

(b) mechanical rotation speed

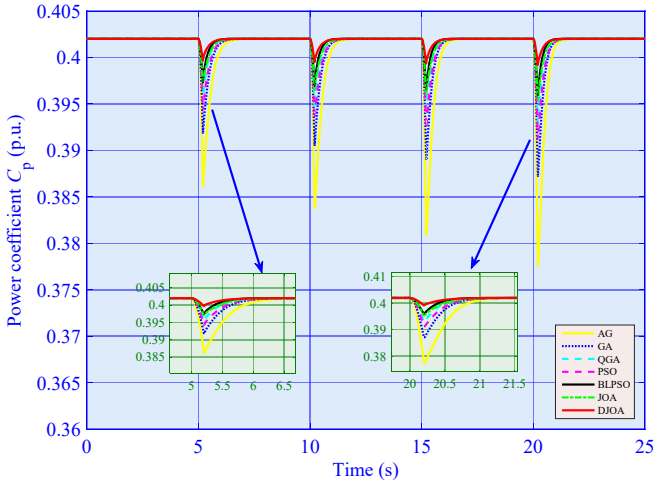

(c) power coefficient

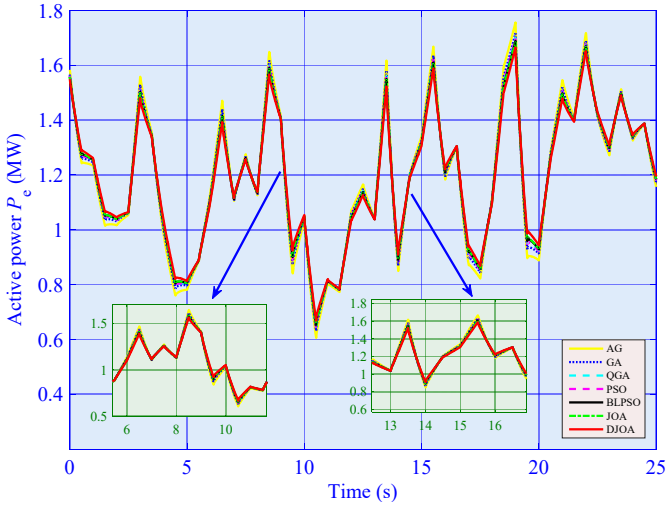

(d) active power

Figure 8: System responses obtained under a low-turbulence stochastic wind speed variation between 7 m/s to 11 m/s.

5.3 High-turbulence stochastic wind speed variation

In order to emulate the fast wind speed variation in some severe cases, e.g., plateau, deserts, coastal areas, etc. [40,41], such severe might influence the stability of the connected power grid [42,43] thus need to be carefully investigated. A high-turbulence stochastic wind speed from 6 m/s to 12 m/s is used to compare the control performance of each algorithm. The system responses are demonstrated in Fig. 9, which clearly shows that DJOA can maintain the power coefficient to be the closest to the optimum in the presence of such rapid wind speed fluctuations. Again, AG performs the worst among all algorithms.

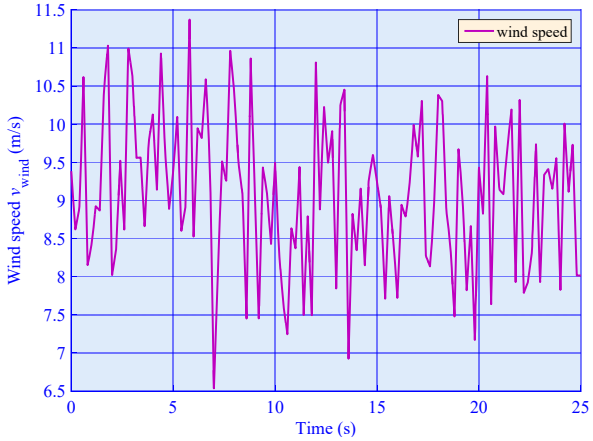

(a) wind speed profile

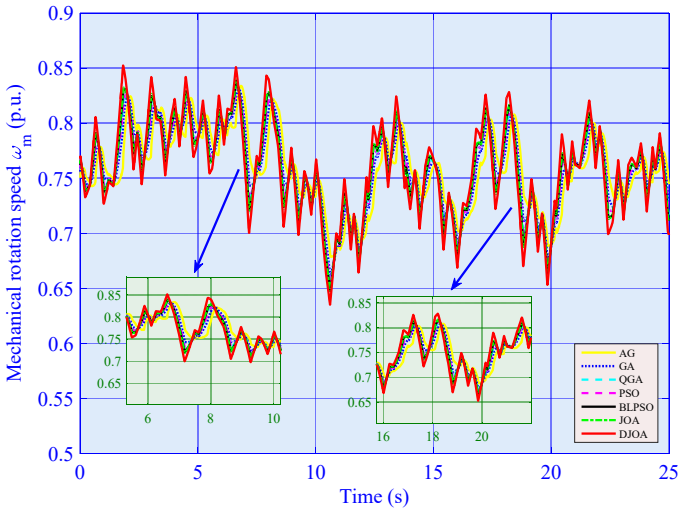

(b) mechanical rotation speed

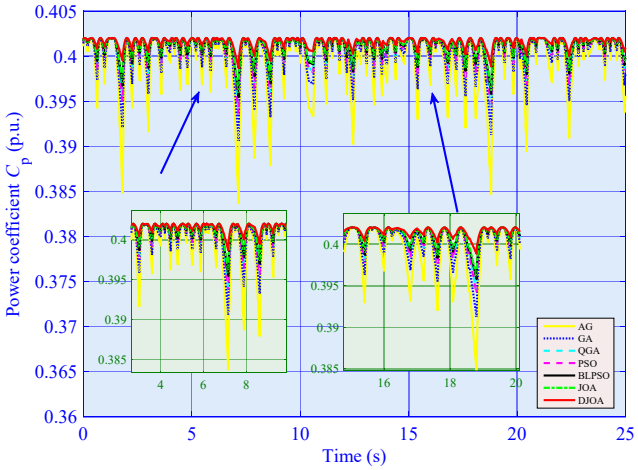

(c) power coefficient

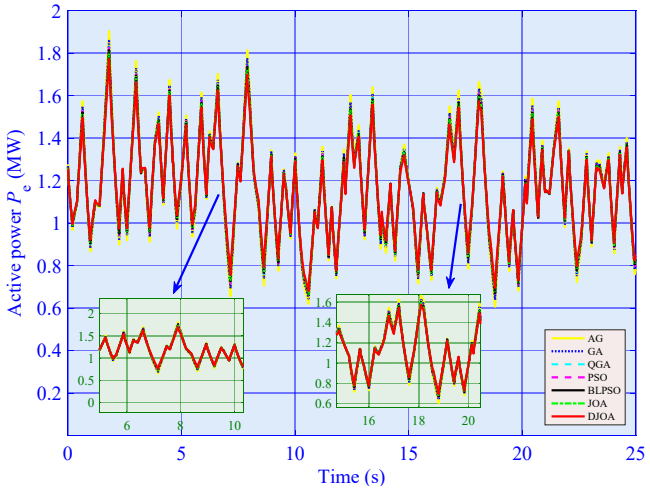

(d) active power

Figure 9: System responses obtained under a high-turbulence stochastic wind speed variation between 6 m/s to 12 m/s.

5.4 Statistic analysis

It is worth noting that all the algorithms are used for offline optimization, not online optimization. In other words, when the optimal PID control parameters are obtained, they will be used in the PID controller. This is due to the fact that the time scale of their execution time (hour) is too long to realize an online optimization of PMSG for MPPT. The offline optimized PID control parameters of different algorithms are tabulated in Table 3, while the meaning of each symbol can be referred in the Nomenclature.

Table 3 The optimal PID control parameters of PMSG obtained by different algorithms in 30 runs.

Algorithm	K_{P1}	K_{I1}	K_{D1}	K_{P2}	K_{I2}	K_{D2}	K_{P3}	K_{I3}	K_{D3}
AG	748.17	630.11	58.47	192.89	56.28	7.76	341.16	254.42	6.21
GA	758.41	542.15	38.25	161.15	79.66	8.98	337.24	253.49	3.53
QGA	761.15	611.32	55.42	194.26	50.26	5.58	361.14	274.42	1.72
PSO	789.24	655.68	90.68	174.57	57.65	7.85	320.14	231.21	2.58
BLPSO	742.68	708.45	93.11	164.56	43.11	9.92	293.54	252.1	5.27
JOA	810.47	485.35	124.72	204.79	98.11	6.79	272.55	191.21	6.28
DJOA	792.15	565.66	149.25	170.09	74.23	6.16	283.57	183.58	8.61

Moreover, the statistical results of execution time, convergence time, and iteration number of convergence are given in Table 4, in which one can observe that the mean execution time, convergence time, and iteration number of convergence of AG are the shortest (highlighted in bold, the same to all the following tables) as it has the simplest optimization mechanism among all the algorithms, while that of DJOA requires relatively longer time due to its more complicated optimization mechanism caused by deeper exploitation and wider exploration. Here, convergence means the first time when an algorithm finds a minimal fitness function in the scheduled maximal iterations.

Table 4 The statistical results of execution time and convergence time obtained by different algorithms in 30 runs.

Algorithm	Execution time (hour)			Convergence time (hour)			Iteration number of convergence		
	Max.	Min.	Mean	Max.	Min.	Mean	Max.	Min.	Mean
AG	**2.13**	**3.41**	**2.77**	**1.86**	**1.21**	**1.54**	**35**	**10**	**23**
GA	21.25	15.14	18.20	5.14	2.28	3.71	127	94	111
QGA	22.41	19.57	20.99	4.55	3.15	3.85	161	132	147
PSO	9.13	6.21	7.67	4.04	1.27	2.66	153	127	140
BLPSO	10.87	6.72	8.80	3.86	1.56	2.71	176	152	164
JOA	11.25	6.34	8.80	5.58	1.94	3.76	185	163	174

DJOA	12.62	6.89	9.76	4.77	2.02	3.40	190	170	180

The integral of absolute error (IAE) indices of different algorithms obtained in three cases are tabulated in Table 5. Here $\mathrm{IAE}_x = \int_0^T |x - x^*| \, \mathrm{d}t$. The simulation time T=25 s is chosen to consider the whole operation range of three cases. It is worth noting that the ideal values of IAE are regarded as the optimal values in this paper, i.e., $\mathrm{IAE}_{\mathrm{Id}}$=0 and $\mathrm{IAE}_{\mathrm{wr}}$=0, which means an ideal control performance (null tacking error). However, such ideal value is impossible to achieve in reality as there always exists some control errors of any type of controllers. Meanwhile, there're no PID control parameters to realize such ideal control performance. One can merely obtain optimal PID control parameters among their boundary to reduce IAE index as much as possible. As provided in Table 5, it can be seen that DJOA offers the smallest IAE indices, thus it can approach the optimal values among all the algorithms. In particular, its $\mathrm{IAE}_{\mathrm{wr}}$ is only 60.12%, 63.60%, 68.59%, 59.56%, 72.14%, and 75.92% of that of AG, GA, QGA, PSO, BLPSO, and JOA in the step change of wind speed. Moreover, its $\mathrm{IAE}_{\mathrm{Id}}$ is just 77.64%, 79.64%, 83.70%, 82.35%, 90.60%, and 90.92% of that of AG, GA, QGA, PSO, BLPSO, and JOA in the high-turbulence stochastic wind speed variation.

Table 5 IAE indices (in p.u.) of different algorithms calculated in three cases in 30 runs.

Cases	IAE Indices	AG	GA	QGA	PSO	BLPSO	JOA	DJOA
Step change of wind speed	$\mathrm{IAE}_{\mathrm{Id}}$	0.2014	0.1862	0.1587	0.1631	0.1427	0.1486	**0.1228**
	$\mathrm{IAE}_{\mathrm{wr}}$	0.3897	0.3684	0.3416	0.3934	0.3248	0.3086	**0.2343**
Low-turbulence stochastic wind speed variation	$\mathrm{IAE}_{\mathrm{Id}}$	0.1903	0.1651	0.1548	0.1872	0.1482	0.1487	**0.1352**
	$\mathrm{IAE}_{\mathrm{wr}}$	0.8124	0.7840	0.7104	0.7395	0.6352	0.6513	**0.5866**
High-turbulence stochastic wind speed variation	$\mathrm{IAE}_{\mathrm{Id}}$	0.2558	0.2314	0.2123	0.2455	0.2018	0.1978	**0.1752**
	$\mathrm{IAE}_{\mathrm{wr}}$	0.9973	0.9722	0.9251	0.9403	0.8546	0.8516	**0.7743**

The overall control costs of different algorithms are depicted in Fig. 10. It can be seen that DJOA just requires the minimal overall control costs in all three cases, which verifies that DJOA can find the global optimum solution with the lowest control costs compared to that of other methods.

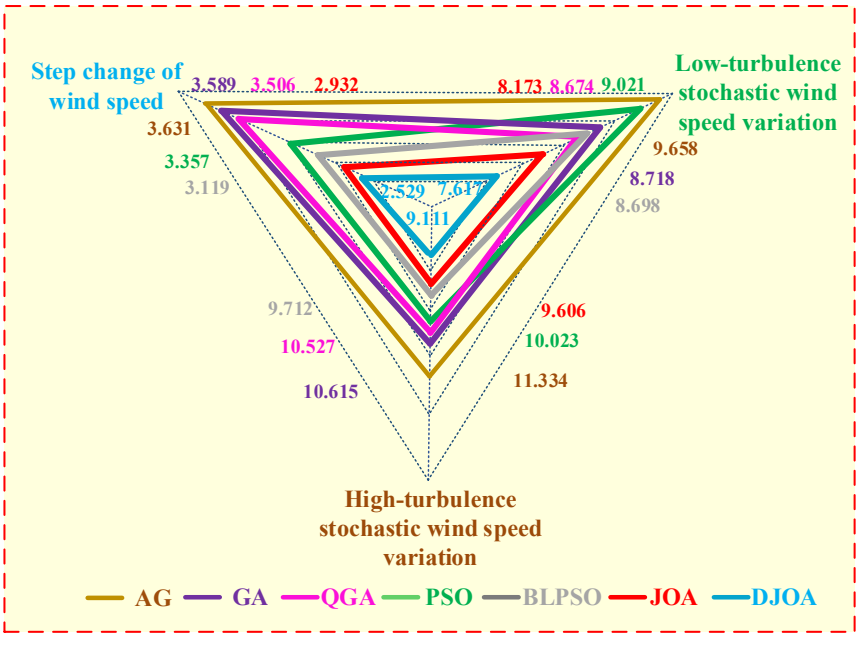

Figure 10. Overall control costs required in three cases of each algorithms.

To this end, Table 6 provides the statistical results of fitness function obtained by different algorithms in 30 runs. Here, the performance indices of DJOA are the lowest among all the algorithms. It is worth noting that the smallest mean value indicates that DJOA can generally find a better optimum with a smaller fitness function, while the lowest standard deviation (Std. Dev.)

and the lowest relative standard deviation (Rel. Std. Dev.) mean the highest convergence stability and reliability. To summarize, DJOA is able to effectively avoid a local optimum due to the combinatorial effect of consensus/compromise between officer and deputy officer in democratic defensive operations and efficient re-organization in shuffling regroup operations, such that it can achieve the most satisfactory global optimum searching.

Table 6 Statistical results of fitness function obtained by different algorithms in 30 runs.

Algorithm	Worst	Best	Mean	Std. Dev.	Rel. Std. Dev.
AG	0.3546	0.2521	0.3034	0.0251	0.0827
GA	0.3264	0.2132	0.2698	0.0233	0.0864
QGA	0.3127	0.2086	0.2607	0.0196	0.0752
PSO	0.2534	0.2018	0.2276	0.0168	0.0738
BLPSO	0.2442	0.1986	0.2214	0.0124	0.0560
JOA	0.2337	0.1946	0.2142	0.0109	0.0509
DJOA	**0.2051**	**0.1815**	**0.1933**	**0.0096**	**0.0497**

6. DISCUSSION

Based on the No Free Lunch theorem, "for any algorithm, any elevated performance over one class of problems is exactly paid for in performance over another class" [47]. It is worth noting that the dimension of the studied PMSG problem is only nine, which is a relatively low-dimensional and simple optimization problem. In order to fully evaluate the performance of DJOA compared to that of other algorithms, such that a biased conclusion toward some chosen problem could be avoided. A set of thirteen standard benchmark functions are employed [48], as tabulated in Table 7, which can be grouped into unimodal functions (f_1 to f_7 with a dimension n=30) and multimodal functions (f_8 to f_{13} with a dimension n=300), respectively. It is our interest to investigate whether the proposed DJOA can be scaled to handle large-scale optimization problem. Hence, multimodal functions (f_8 to f_{13}), for which the number of their local minima increases exponentially with respect to the increase of dimension, as selected and extended to 300 dimensions.

The same algorithm parameters used in the case studies are adopted while the tolerance of convergence error ε=10^{-10}. 300 independent runs are executed on each algorithm while their results are averaged and listed in Table 8, in which the CPU time unit is in second. From Table 8, it shows that DJOA can outperform other algorithms in high-dimensional multimodal functions (f_8 to f_{13}) thanks to its unique shuffling regroup operations and democratic defensive operations. Although BLPSO or QGA outperforms DJOA in some cases (f_1-f_3, f_5), DJOA can still obtain a relative satisfactory optimization with just similar results to those which performs the best. At last, it can conclude that DJOA usually consumes the longest time for optimization resulted from its complicated searching mechanism.

Table 7 Thirteen benchmark functions, where n is the dimension of the function, and $f_{\min}$ is the global minimum value of the function.

Test benchmark functions	n	S	$f_{\min}$
$f_1(x)=\sum_{i=1}^{n} x_i^2$	30	$[-100,100]^n$	0
$f_2(x)=\sum_{i=1}^{n}\lvert x_i\rvert+\prod_{i=1}^{n}\lvert x_i\rvert$	30	$[-10,10]^n$	0
$f_3(x)=\sum_{i=1}^{n}\left(\sum_{j=1}^{n} x_j\right)^2$	30	$[-100,100]^n$	0
$f_4(x)=\max_i\{\lvert x_i\rvert, 1\le i\le n\}$	30	$[-100,100]^n$	0
$f_5(x)=\sum_{i=1}^{n-1}(100(x_{i+1}-x_i^2)^2+(x_i-1))^2$	30	$[-30,30]^n$	0
$f_6(x)=\sum_{i=1}^{n}(\lfloor x_i+0.5\rfloor)^2$	30	$[-100,100]^n$	0
$f_7(x)=\sum_{i=1}^{n} ix_i^4+\mathrm{random}[0,1)$	30	$[-1.28,1.28]^n$	0
$f_8(x)=-\sum_{i=1}^{n}\left(x_i\sin\left(\sqrt{\lvert x_i\rvert}\right)\right)$	300	$[-500,500]^n$	-125694.7
$f_9(x)=\sum_{i=1}^{n}(x_i^2-10\cos(2\pi x_i)+10)^2$	300	$[-5.12,5.12]^n$	0
$f_{10}(x)=-20\exp\left(-0.2\sqrt{\frac{1}{n}\sum_{i=1}^{n}x_i^2}\right)-\exp\left(\frac{1}{n}\sum_{i=1}^{n}\cos 2\pi x_i\right)+20+e$	300	$[-32,32]^n$	0
$f_{11}(x)=\frac{1}{4000}\sum_{i=1}^{30}(x_i-100)^2-\prod_{i=1}^{n}\cos\left(\frac{x_i-100}{\sqrt{i}}\right)+1$	300	$[-600,600]^n$	0
$f_{12}(x)=\frac{\pi}{n}\{10\sin^2(\pi y_1)+\sum_{i=1}^{29}(y_i-1)^2[1+10\sin^2(\pi y_{i+1})]+(y_n-1)^2\}+\sum_{i=1}^{30}u(x_i,10,100,4)$ $y_i=1+\frac{1}{4}(x_i+1)$	300	$[-50,50]^n$	0

$u(x_i,a,k,m)=\begin{cases}k(x_i-a)^m, & x_i>a\\ 0, & -a\le x_i\le a\\ k(-x_i-a)^m, & x_i<-a\end{cases}$			
$f_{13}(x)=0.1\{\sin^2(\pi 3x_1)+\sum_{i=1}^{29}(x_i-1)^2[1+\sin^2(3\pi x_{i+1})]+(x_n-1)^2[1+\sin^2(2\pi x_{30})]\}+\sum_{i=1}^{30}u(x_i,5,100,4)$	300	$[-50,50]^n$	0

Table 8 Comparison of DJOA with AG, GA, QGA, PSO, BLPSO, JOA, and DJOA on benchmark function f_1-f_{13}.All results have averaged over 200 runs

Function	Algorithms	Mean	Std.	CPU(s)	Function	Algorithms	Mean	Std.	CPU(s)
f_1	AG	1.341	0.569	6.751	f_8	AG	-9782.427	35.175	10.579
	GA	0.067	0.013	14.125		GA	-10681.183	1.793	18.306
	QGA	5.677×10^{-7}	2.041×10^{-7}	21.384		QGA	-11567.247	3.175	22.479
	PSO	3.213×10^{-9}	2.142×10^{-9}	40.293		PSO	-10403.938	40.492	47.732
	BLPSO	2.896×10^{-9}	1.683×10^{-9}	44.257		BLPSO	-11184.271	28.428	52.279
	JOA	1.627×10^{-8}	1.360×10^{-8}	30.001		JOA	-10895.523	1.783×10^{-2}	33.543
	DJOA	1.139×10^{-8}	9.522×10^{-9}	36.471		DJOA	-12046.866	1.249×10^{-2}	39.754
f_2	AG	0.713	0.241	5.972	f_9	AG	2.873	0.897	12.573
	GA	0.491	0.111	14.803		GA	0.553	0.306	29.662
	QGA	5.974×10^{-2}	2.207×10^{-2}	23.688		QGA	0.499	0.426	35.179
	PSO	2.537×10^{-10}	9.885×10^{-10}	42.735		PSO	1.084	0.972	79.254
	BLPSO	1.026×10^{-10}	3.155×10^{-10}	46.153		BLPSO	0.687	0.749	86.271
	JOA	3.092×10^{-5}	7.196×10^{-5}	29.523		JOA	0.850	0.794	54.459
	DJOA	2.165×10^{-5}	5.037×10^{-5}	34.675		DJOA	0.595	0.526	59.905
f_3	AG	8.988	5.167	5.587	f_{10}	AG	2.749	0.974	9.267
	GA	8.427	2.715	14.464		GA	0.738	0.238	21.809
	QGA	6.971	2.189	18.716		QGA	0.157	0.067	27.834
	PSO	2.042	0.837	40.404		PSO	1.163×10^{-1}	3.689×10^{-1}	48.951
	BLPSO	1.743	0.772	46.217		BLPSO	7.893×10^{-2}	1.267×10^{-2}	57.833
	JOA	4.829	2.074	26.632		JOA	2.259×10^{-3}	2.572×10^{-3}	37.396
	DJOA	3.380	1.152	29.295		DJOA	1.532×10^{-5}	1.879×10^{-5}	41.134
f_4	AG	1.203	0.342	4.663	f_{11}	AG	2.347	0.387	6.197
	GA	0.767	0.281	13.673		GA	0.653	5.741×10^{-2}	18.193
	QGA	0.572	0.311	18.106		QGA	1.543×10^{-1}	7.145×10^{-2}	31.849
	PSO	0.359	0.218	30.737		PSO	0.202	0.085	50.394
	BLPSO	0.122	2.984×10^{-2}	35.287		BLPSO	9.968×10^{-2}	2.427×10^{-2}	73.873
	JOA	0.095	3.338×10^{-2}	39.784		JOA	2.576×10^{-2}	1.067×10^{-2}	39.023
	DJOA	6.301×10^{-2}	2.337×10^{-2}	32.762		DJOA	1.794×10^{-5}	8.8046×10^{-6}	49.927
f_5	AG	102.354	27.468	4.024	f_{12}	AG	0.519	0.087	9.637
	GA	87.721	30.273	12.769		GA	3.705×10^{-2}	4.291×10^{-2}	26.216
	QGA	27.736	26.287	17.524		QGA	7.247×10^{-3}	1.873×10^{-3}	38.790
	PSO	32.502	17.965	41.736		PSO	3.436×10^{-1}	7.954×10^{-1}	49.728
	BLPSO	21.037	14.287	48.798		BLPSO	5.187×10^{-2}	1.034×10^{-2}	53.692
	JOA	41.613	25.198	30.219		JOA	2.301×10^{-7}	7.652×10^{-8}	37.395
	DJOA	29.129	17.638	33.241		DJOA	6.613×10^{-10}	3.354×10^{-10}	46.131
f_6	AG	5.186	2.103	7.279	f_{13}	AG	1.428	0.893	10.392
	GA	3.142	1.659	13.891		GA	0.657	6.008×10^{-1}	25.538
	QGA	2.237	1.176	17.242		QGA	0.089	3.264×10^{-2}	43.276
	PSO	0.127	0.364	43.179		PSO	0.479	1.738×10^{-1}	50.505
	BLPSO	0.086	0.127	46.217		BLPSO	0.037	1.579×10^{-2}	61.872
	JOA	0.013	0.004	29.458		JOA	3.921×10^{-3}	5.844×10^{-3}	46.697
	DJOA	9.352×10^{-3}	0.078	32.404		DJOA	2.744×10^{-7}	4.092×10^{-8}	68.562
f_7	AG	0.164	0.051	5.183					
	GA	0.084	0.031	13.786					
	QGA	0.127	0.046	15.277					
	PSO	0.086	0.032	45.954					

	BLPSO	0.047	0017	48.178	
	JOA	0.062	7.726×10^{-2}	34.132	
	DJOA	0.043	5.410×10^{-2}	37.545	

7. CONCLUSION

This paper proposes a novel DJOA for the optimal PID control parameters tuning of PMSG based WECS, such that the optimal wind energy can be extracted under various wind speed profiles. The main findings and conclusions of this paper can be summarized as follows:

(1) Inspired by the military philosophy, three essential strategies, e.g., offensive operations, democratic defensive operations, and shuffling regroup operations, are adopted to balance the trade-off between global exploration and local exploitation, together with the ability of local optimum avoidance;

(2) The democratic defensive operation is formed via introducing an additional deputy officer into each military unit. Based on the consensus/compromise between the officer and deputy officer, a deeper optimum search can be realized;

(3) The shuffling regroup operations is proposed based on shuffling strategy of SFLA, which can significantly enhance the local optimum avoidance ability through global position information sharing among all the soldiers;

(4) DJOA is applied on PMSG based WECS for the optimal MPPT as an interdisciplinary study of wind energy conversion, control, and optimization. Simulation results demonstrate that DJOA owns the lowest tracking error and control costs compared to that of AG, GA, QGA, PSO, BLPSO, and JOA.

Future study will be focused on the following two aspects:

(a) Apply DJOA on grid-side VSC controller for fault ride-through (FRT) capability enhancement, together with the generator-side VSC controller presented in this paper, such that a complete DJOA design for PMSG based WECS will be accomplished;

(b) Use DJOA to optimizer the control parameters of fractional-order PID controller so as to further improve the control performance;

(c) Comprehensively investigate the optimization performance of DJOA for complicated mathematical optimization problems, such as constrained optimization, large-scale optimization, multi-objective optimization.

Acknowledgement

The authors gratefully acknowledge the support of National Natural Science Foundation of China (51477055, 51667010, 51777078), and Scientific Research Foundation of Yunnan Provincial Department of Education (2017ZZX146).

References

[1] Liao SW, Yao W, Han XN, Wen JY, Cheng SJ. Chronological operation simulation framework for regional power system under high penetration of renewable energy using meteorological data. *Applied Energy* **2017**; 203: 816-828.

[2] Yang B, Zhang XS, Yu T, Shu HC, Fang ZH. Grouped grey wolf optimizer for maximum power point tracking of doubly-fed induction generator based wind turbine. *Energy Conversion and Management* **2017**; 133: 427-443.

[3] Fathabadi H. Novel high efficient speed sensorless controller for maximum power extraction from wind energy conversion systems. *Energy Conversion and Management* **2016**, 123, 392-401.

[4] Liu J, Wen JY, Yao W, Long Y. Solution to short-term frequency response of wind farms by using energy storage systems. *IET Renewable Power Generation* **2016**; 10(5): 669-678.

[5] Yang B, Jiang L, Wang L, Yao W, Wu QH. Nonlinear maximum power point tracking control and modal analysis of DFIG based wind turbine. *International Journal of Electrical Power and Energy Systems* **2016**; 74: 429-436.

[6] Li SH, Haskew TA, Xu L. Conventional and novel control designs for direct driven PMSG wind turbines. *Electric Power Systems Research* **2010**; 80: 328-338.

[7] Beddar A, Bouzekri H, Babes B, Afghoul H. Experimental enhancement of fuzzy fractional order PI+I controller of grid connected variable speed wind energy conversion system. *Energy conversion and management* **2016**, 123:569-580.

[8] Yin XX, Lin YG, Li W, Gu YJ, Liu HW, Lei PF. A novel fuzzy integral sliding mode current control strategy for maximizing wind power extraction and eliminating voltage harmonics. *Energy* **2015**; 85: 677-686.

[9] Khalil HK. Nonlinear systems third edition. Upper Saddle River, NJ: Prentice-Hall, Inc., 2002.

[10] Chen J, Jiang L, Yao W, Wu QH. A feedback linearization control strategy for maximum power point tracking of a PMSG based wind turbine. *International Conference on Renewable Energy Research and Applications*, Madrid, Spain, 20-23 October 2013, 79-84.

[11] Youcef S, Sami K, Mohcene B. Feedback linearization control based particle swarm optimization for maximum power point tracking of wind turbine equipped by PMSG connected to the grid. *International Journal of Hydrogen Energy* **2016**; 41: 20950-20955.

[12] Seyed MM, Maarouf S, Hani V, Handy FB, Mohsen S. Sliding mode control of PMSG wind turbine based on enhanced exponential reaching law. *IEEE Transactions on Industrial Electronics* **2016**; 63(10): 6148-6159.

[13] Fantino R, Solsona J, Busada C. Nonlinear observer-based control for PMSG wind turbine. *Energy* **2016**; 113: 248-257.

[14] Wei C, Zhang Z, Qiao W, Qu LY. An adaptive network-based reinforcement learning method for MPPT control of PMSG wind energy conversion systems. *IEEE Transactions on Power Electronics* **2016**; 31(11): 7837-7848.

[15] Errami Y, Ouassaid M, Cherkaoui M, Maaroufi M. Maximum power point tracking control based on a nonlinear backstepping approach for a permanent magnet synchronous generator wind energy conversion system connected to a utility grid. *Energy Technology* **2015**; 3(7): 743-757.

[16] Li SQ, Zhang KZ, Li J, Liu C. On the rejection of internal and external disturbances in a wind energy conversion system with direct-driven PMSG. *ISA Transactions* **2016**; 61: 95-103.

[17] Xing B, Gao WJ. Innovative computational intelligence: A rough guide to 134 clever algorithms. Springer International Publishing, Switzerland, 2014.

[18] Hasanien HM, Muyeen SM. Design optimization of controller parameters used in variable speed wind energy conversion system by genetic algorithms. *IEEE Transactions on Sustainable Energy* **2012**; 3(2): 200-208.

[19] Kim YS, Chung IY, Moon SI. Tuning of the PI controller parameters of a PMSG wind turbine to improve control performance under various wind speeds. *Energies* **2015**; 8(2): 1406-1425.

[20] Rukslin, Haddin M, Suprajitno A. Pitch angle controller design on the wind turbine with permanent magnet synchronous generator (PMSG) base on firefly algorithms (FA). *Technology of Information and Communication. IEEE*, 2017: 13-17.

[21] Hong CM, Cheng FS, Chen CH. Optimal control for variable-speed wind generation systems using general regression neural network. *International Journal of Electrical Power and Energy Systems* **2014**; 60: 14-23.

[22] Niknam T, Taheri SI, Aghaei J, Tabatabaei S, Nayeripour M. A modified honey bee mating optimization algorithm for multiobjective placement of renewable energy resources. *Applied Energy* **2011**; 88(12): 4817-4830.

[23] Guirguis D, Romero DA, Amon CH. Gradient-based multidisciplinary design of wind farms with continuous-variable formulations. *Applied Energy* **2017**; 197: 279-291.

[24] Chen H, Zhang R, Li G, Bai L. Economic dispatch of wind integrated power systems with energy storage considering composite operating costs. *IET Generation Transmission & Distribution* **2016**; 10(5): 1294-1303.

[25] Sun GJ, Zhao RQ, Lan YF. Joint operations algorithm for large-scale global optimization. *Applied Soft Computing* **2016**; 38: 1025-1039.

[26] Eusuff M, Lansey K, Pasha F. Shuffled frog-leaping algorithm: a memetic meta-heuristic for discrete optimization. *Engineering Optimization* **2006**; 38(2): 129-154.

[27] Sharmaa TK, Pant M. Opposition based learning ingrained shuffled frog-leaping algorithm. *Journal of Computational Science* **2017**; 21: 307-315.

[28] Chen J, Jiang L, Yao W, Wu QH. Perturbation estimation based nonlinear adaptive control of a full-rated converter wind turbine for fault

ride-through capability enhancement. *IEEE Transactions on Power Systems* **2014**; 29(6): 2733-2743.

[29] Uehara A, Pratap A, Goya T, Senjyu T, Yona A, Urasaki N, Funabashi T. A coordinated control method to smooth wind power fluctuations of a PMSG-based WECS. *IEEE Transactions on Energy Conversion* **2011**; 26(2): 550-558.

[30] Yang B, Hu YL, Huang HY, Shu HC, Yu T, Jiang L. Perturbation estimation based robust state feedback control for grid connected DFIG wind energy conversion system. *International Journal of Hydrogen Energy* **2017**; 42(33): 20994-21005.

[31] Yang B, Yu T, Shu HC, Dong J, Jiang L. Robust sliding-mode control of wind energy conversion systems for optimal power extraction via nonlinear perturbation observers. *Applied Energy*. http://dx.doi.org/10.1016/j.apenergy.2017.08.027

[32] Amegashie JA. Regime spoiler or regime pawn: The military and distributional conflict in non-democracies. *Journal of Comparative Economics* **2015**; 43: 491-502.

[33] Acemoglu D, Ticchi D, Vindigni A. A theory of military dictatorships. *American Economic Journal Macroeconomics* **2010**; 2(1): 1-42.

[34] Lee J. Indifferentiability of the sum of random permutations towards optimal security. *IEEE Transactions on Information Theory* **2017**; 63(6): 4050-4054.

[35] Wu FJ, Sun DY, Duan JD. Diagnosis of single-phase open-line fault in three-phase PWM rectifier with LCL filter. *IET Generation Transmission & Distribution* **2016**; 10(6): 1410-1421.

[36] Fang KT, Zhang Y. Uniform design: theory and application. *Technometrics* **2000**; 42(3): 237-248.

[37] Kazemtabrizi B, Acha E. An advanced STATCOM model for optimal power flows using Newton's method. *IEEE Transactions on Power Systems* **2014**, 29(2): 514-525.

[38] Wang MQ, Gooi HB, Chen SX, S Lu. A mixed integer quadratic programming for dynamic economic dispatch with value pint effect. *IEEE Transactions on Power Systems* **2014**, 29 (5):2097-2106.

[39] Duan C, Fang W, Jiang L, Liu J. Adaptive barrier filter-line-search interior point method for optimal power flow with FACTS devices, *IET Generation, Transmission & Distribution* **2015**, 9 (16): 2792–2798.

[40] Mi XW, Liu H, Li YF. Wind speed forecasting method using wavelet, extreme learning machine and outlier correction algorithm. *Energy Conversion and Management* **2017**; 151: 709-722.

[41] Shen Y, Yao W, Wen JY, He HB. Adaptive wide-area power oscillation damper design for photovoltaic plant considering delay compensation. *IET Generation, Transmission & Distribution*, DOI: 10.1049/iet-gtd.2016.2057.

[42] Yao W, Jiang L, Wen JY, Wu QH, Cheng SJ. Wide-are damping controller for power system inter-area oscillations: a network predictive control approach. *IEEE Transactions on Control Systems Technology* **2015**; 23(1): 27-36.

[43] Shen Y, Yao W, Wen JY, He HB, Chen WB. Adaptive supplementary damping control of VSC-HVDC for interarea oscillation using GrHDP. *IEEE Transactions on Power Systems*, DOI: 10.1109/TPWRS.2017.2720262.

[44] Malossini A, Blanzieri E, Calarco T. Quantum genetic optimization. *IEEE Transactions on Evolutionary Computation* **2008**; 12(2): 231-241.

[45] Chen X, Tianfield H, Mei C, Du W, Liu G. Biogeography-based learning particle swarm optimization. *Soft Computing* **2017**; 21: 7519-7541.

[46] D'Aspremont A. Smooth optimization with approximate gradient. *Siam Journal on Optimization* **2008**, 19(3):1171-1183.

[47] Wolpert DH, Macready WG, No free lunch theorems for search. *IEEE Transactions on Evolution Computation* **1997**; 1(1): 67-82.

[48] Yao X, Liu Y, Liu G. Evolutionary programming made faster. *IEEE Transactions on Evolution Computation* **1999**; 3(2): 82-102.